Available online at www.sciencedirect.com
ScienceDirect
Nuclear Physics B Proceedings Supplement 00 (2014) 1–5
Nuclear Physics B Proceedings Supplement

Study of Baryon Production at Belle and BABAR

Min-Zu Wang on behalf of the Belle and BABAR Collaboration

Department of Physics, Institute of Astrophysics and Leung Center for Cosmology and Particle Astrophysics, National Taiwan University, Taiwan, R.O.C.

Abstract

Recent results related to baryon productions with the full data set collected by Belle or BABAR are shown. These include inclusive antideuteron production at $\Upsilon(nS)$, branching fraction measurement of $\Lambda_c^+ \to pK^-\pi^+$, precision measurements of the masses and widths of $\Sigma_c(2455)^{0/++}$ and $\Sigma_c(2520)^{0/++}$, searches for doubly charmed baryons/charmed strange baryons, and exclusive $\Lambda\bar{\Lambda}$ production at$\Upsilon(1S, 2S)$.

Keywords: baryon, production, Belle, BABAR, inclusive, antideuteron, charmed

1. Inclusive antideuteron production at $\Upsilon(nS)$ [1]

It is of general interests to search for antideuterons in the outer space as a probe for dark matter annihilation or anti-matter world. Previous experiments showed that antideuterons can be produced in Υ decays which was quite unexpected due to a much larger kinetic energy of the valence quarks comparing with the nuclear binding energy. Precise measurements of the related production rates and momentum spectra are useful to understand the production mechanism.

The BABAR collaboration used the data samples collected near $\Upsilon(2S)$, $\Upsilon(3S)$ and $\Upsilon(4S)$ to study antideuteron production. Signal yield is estimated with the fit to the normalized residuals of the dE/dx information for antideuteron candidates, as shown in Fig. 1 . The yields of the inclusive antideuteron production in $\Upsilon(2S)$, $\Upsilon(3S)$ and $\Upsilon(4S)$ decays can be obtained by subtracting the properly rescaled yields in the Offpeak datasets from yields in the Onpeak ones. The number of $\bar{d}$'s is compatible with zero for $\Upsilon(4S)$. We concluded that the production of antideuteron is mainly via the $e^+e^- \to q\bar{q}$ process near $\Upsilon(4S)$. To extract the signal yield in $\Upsilon(1S)$ decays, we used the $\pi^+\pi^-$ recoil mass spectrum of the $\Upsilon(2S)$ dataset to identify $\Upsilon(1S)$ candidates from $\Upsilon(2S) \to \Upsilon(1S)\pi^+\pi^-$. The measured results are summarized in Table 1. It is interesting to note that the $\bar{d}$ production rate is highly suppressed in quark-dominated $e^+e^- \to q\bar{q}$ comparing to the gluon-dominated $\Upsilon(1S, 2S, 3S)$ decays.

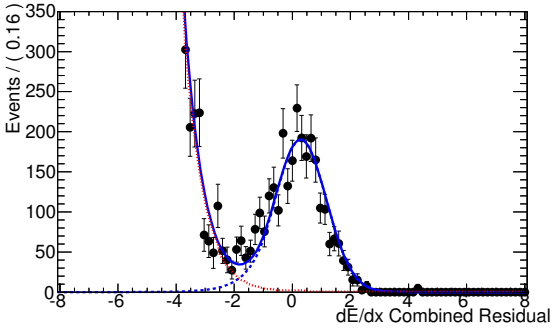

Figure 1: Normalized residuals of the combined dE/dx for antideuteron candidates in the Onpeak $\Upsilon(2S)$ data sample, with fit p.d.f.'s superimposed. Entries have been weighted with the related efficiencies from Monte Carlo (MC)simulation. The solid (blue) line is the total fit, the dashed (blue) line is the $\bar{d}$signal peak, and the dotted (red) line is the background.

The momentum spectra of produced $\bar{d}$'s are useful for theoretical investigation. As an illustration, Fig. 2 shows the momentum spectrum of $\bar{d}$'s in $\Upsilon(2S) \to \bar{d}X$ and a fit to the fireball model [3].

Table 1: Total rates of antideuteron production. The first uncertainties listed are statistical, the second systematic. For comparison, we also list the ratio of our measurement of the inclusive antideuteron cross section to the cross section for hadronic production at a similar energy evaluated from [2]. Here we only quote our own uncertainties, the hadronic cross section itself has a 7% uncertainty.

Process	Rate
$\mathcal{B}(\Upsilon(3S) \to \bar{d}X)$	$(2.33 \pm 0.15^{+0.31}_{-0.28}) \times 10^{-5}$
$\mathcal{B}(\Upsilon(2S) \to \bar{d}X)$	$(2.64 \pm 0.11^{+0.26}_{-0.21}) \times 10^{-5}$
$\mathcal{B}(\Upsilon(1S) \to \bar{d}X)$	$(2.81 \pm 0.49^{+0.20}_{-0.24}) \times 10^{-5}$
$\sigma(e^+e^- \to \bar{d}X) \sim \Upsilon(4S)$	$(9.63 \pm 0.41^{+1.17}_{-1.01})$ fb
$\frac{\sigma(e^+e^- \to \bar{d}X)}{\sigma(e^+e^- \to \text{Hadrons})}$	$(3.01 \pm 0.13^{+0.37}_{-0.31}) \times 10^{-6}$

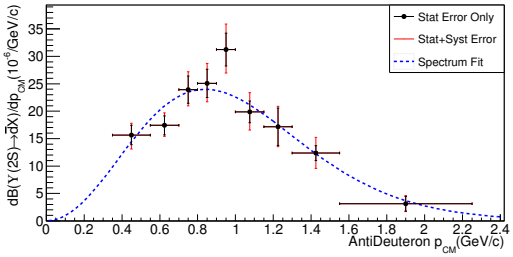

Figure 2: Measured antideuteron differential spectra in $\Upsilon(2S)$ decays. The points with inner (black) error bars give the measurements and their associated statistical uncertainties, the outer (red) error bars give the quadratic sum of the statistical and systematic uncertainties, and the dashed (blue) curves show the fit to the functional form based on the fireball model.

2. Branching fraction measurement of $\Lambda_c^+ \to pK^-\pi^+$ [4]

The decay process $\Lambda_c^+ \to pK^-\pi^+$ [5] is the most common mode used to tag the charmed baryon in the study of flavor physics. It is also the calibration mode for branching fraction measurements of the Λ_c^+ decays. However, the old world average [6] is $\mathcal{B}(\Lambda_c^+ \to pK^-\pi^+) = (5.0 \pm 1.3)\%$ with a large uncertainty. The Belle collaboration used a 978 fb^{-1}data sample to pursue a model-independent measurement of the absolute branching fraction of $\Lambda_c^+ \to pK^-\pi^+$.

We use this missing mass spectrum of $D^{(*)-}\overline{p}\pi^+$ from $e^+e^- \to D^{(*)-}\overline{p}\pi^+\Lambda_c^+$ to determine the inclusively tagged Λ_c^+ yield. Only twelve decay modes from D decays are reconstructed. The D^* candidates are selected by combining the D candidate and a slow pion with a proper $D*$ mass. To ensure there is no random peaking background, we compare the right sign (RS) $D^{(*)-}\overline{p}\pi^+$ sample with the wrong sign (WS) sample, namely $D^{(*)-}p\pi^-$ and $D^{(*)+}\overline{p}\pi^-$. The results are shown in Fig. 3

We use the inclusively tagged Λ_c^+ sample to positively

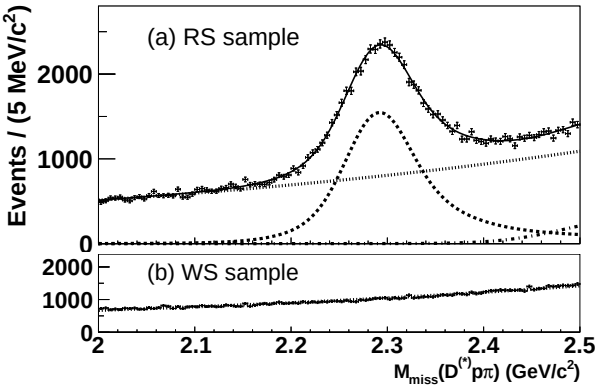

Figure 3: The $M_{\rm miss}(D^{(*)}p\pi)$ data distributions (points with error bars) for inclusively reconstructed Λ_c^+ baryons from the (a) RS and (b) WS samples with superimposed fit results (solid line). The contributions of signal, combinatorial and missing $D^{(*)-}\overline{p}\pi^+\Lambda_c^+X$ background are shown with the dashed, dotted, and dashed-dotted lines, respectively.

reconstruct $\Lambda_c^+ \to pK^-\pi^+$ signals, shown in Fig. 4. Background subtraction is performed using the inclusive Λ_c^+ yields in the pre-defined signal region and sideband region. The branching fraction of the $\Lambda_c^+ \to pK^-\pi^+$ decay is given by

$$\mathcal{B}(\Lambda_c^+ \to pK^-\pi^+) = \frac{N(\Lambda_c^+ \to pK^-\pi^+)}{N_{\rm inc}^{\Lambda_c} f_{\rm bias} \varepsilon(\Lambda_c^+ \to pK^-\pi^+)} \quad (1)$$

where $N_{\rm inc}^{\Lambda_c}$ denotes the number of inclusively reconstructed Λ_c^+ baryons, $N(\Lambda_c^+ \to pK^-\pi^+)$ is the number of reconstructed $\Lambda_c^+ \to pK^-\pi^+$ decays found in the inclusive Λ_c^+ sample, $\varepsilon(\Lambda_c^+ \to pK^-\pi^+)$ represents the reconstruction efficiency of $\Lambda_c^+ \to pK^-\pi^+$ decays within the inclusive Λ_c^+ sample, and $f_{\rm bias}$ is a correction factor $\sim$ 1 which takes into account the dependence of the inclusive Λ_c^+ reconstruction efficiency on the Λ_c^+ decay mode. The measured branching fraction is $\mathcal{B}(\Lambda_c^+ \to pK^-\pi^+) = (6.84 \pm 0.24^{+0.21}_{-0.27})\%$ which represents a fivefold improvement in precision comparing with the old world average [6].

3. Precision measurements of the masses and widths of $\Sigma_c(2455)^{0/++}$ and $\Sigma_c(2520)^{0/++}$ [7]

Many theoretical frameworks (e.g. lattice QCD, heavy quark effective theory, quark model, QCD sum rule, bag model, etc.) are established to describe or predict properties of hadrons. These properties in general cannot be calculated by QCD due to the non-perturbative limitation at low energy scale. The masses and widths of the $\Sigma_c^{0/++}$ baryons have been measured

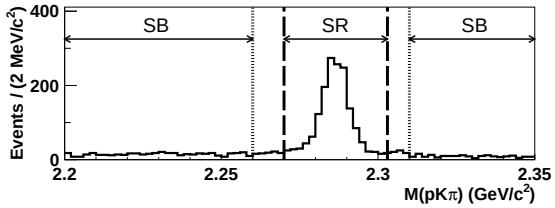

Figure 4: The $M(pK\pi)$ distribution of exclusively reconstructed $\Lambda_c^+ \to pK^-\pi^+$ candidates within the inclusive Λ_c^+ sample. The dashed (dotted) vertical lines indicate the borders of signal (SR) and sideband (SB) regions.

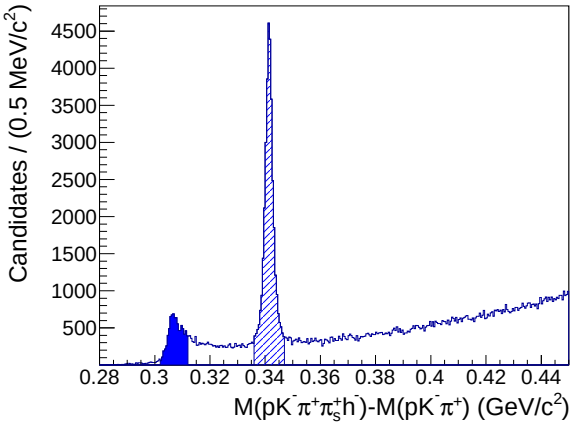

Figure 5: Mass difference of $M(pK^-\pi^+\pi_s^+h^-) - M(pK^-\pi^+)$. Tagged events falling in the regions of the $\Lambda_c(2595)^+$ (filled) and $\Lambda_c(2625)^+$ (hatched) are properly weighted and subtracted in the mass difference plot of $M(pK^-\pi^+\pi_s^+) - M(pK^-\pi^+)$.

by many experiments with a bit large uncertainties [6]. Due to the mass hierarchy between the d and u quarks, Naively people would guess that the Σ_c^0 (ddc) baryon should be heavier than the Σ_c^{++} (uuc) baryon due to the constituent valence quarks; however, the experimental results contradict this expectation. To explain the discrepancy, various models have been introduced and predict the mass splittings. Precise measurements of the mass splittings are necessary to test these models.

The Belle collaboration used a data sample corresponding to an integrated luminosity of 711 fb^{-1} to perform such measurements. The $\Sigma_c^{0/++}$ baryons are reconstructed via the $\Sigma_c^{0/++} \to \Lambda_c^+(\to pK^-\pi^+)\pi_s^{-/+}$ decay channel, where π_s denotes a slow pion. To remove the feed-down background from excited Λ_c^+ baryons, we add one extra track (h) with opposite charge against π_s to check the reconstructed mass difference between excited Λ_c^+ and Λ_c^+. For example, the mass difference of $M(pK^-\pi^+\pi_s^+h^-) - M(pK^-\pi^+)$ is shown in Fig. 5. Clear $\Lambda_c(2595)^+$ and $\Lambda_c(2625)^+$ signals are seen. The excited Λ_c^+ candidates are properly weighted and subtracted in the mass difference plots of $M(pK^-\pi^+\pi_s^-) - M(pK^-\pi^+)$ and $M(pK^-\pi^+\pi_s^+) - M(pK^-\pi^+)$, shown in Fig. 6.

We use binned maximum likelihood fits in Fig. 6 to determine the mass splittings and widths of $\Sigma_c(2455)^{0/++}$ and $\Sigma_c(2520)^{0/++}$. The signal shapes are described by a relativistic Breit-Wigner function convolved with the detector response function. The random background without a true Λ_c^+ is estimated from the Λ_c^+ mass sideband. The random background with a true Λ_c^+ is modeled by a threshold function. The fit results are shown in table 2. Detailed studies on background subtraction, background validation, momentum calibration, detector resolution, fitting procedure....are carried out in order to obtain the systematical uncertainties. These measurements represent the most precise values to date.

4. Searches for doubly charmed baryons/charmed strange baryons [8]

The hadron spectroscopy is well established in the single-charmed baryon sector. However there are no doubly-charmed baryons being observed experimentally except the evidence reported by the SELEX collaboration for the Ξ_{cc}^+ baryon. The lightest doubly-charmed baryon consists of two charm quarks and one up or down quark ($\Xi_{cc}^+ = ccd$, $\Xi_{cc}^{++} = ccu$). The mass of the Ξ_{cc} has been extensively studied theoretically and is predicted in the range from 3.48 GeV/c^2 to 3.74 GeV/c^2.

Both the Belle and BaBar collaboration searched for the $\Xi_{cc}^{+(+)}$ before and found no evidence. Upper limit on the product of the production cross section and branching fractions of Ξ_{cc} was set depending on the decay mode. It is at a few fb level.

The Belle collaboration reported an improved search for the Ξ_{cc} in its weak decays to the $\Lambda_c^+K^-\pi^+(\pi^+)$ and $\Xi_c^0\pi^+(\pi^+)$ final states using a data sample with a total integrated luminosity of 980 fb^{-1}. The same data sample was also used to study charmed strange baryons since the excited Ξ_c^+ (Ξ_c^{*+}) states can decay to $\Lambda_c^+K^-\pi^+$ and $\Xi_c^0\pi^+$.

We only present the results for the $\Lambda_c^+K^-\pi^+(\pi^+)$ final state here. The Λ_c^+ is reconstructed in the $pK^-\pi^+$ and pK_S^0 decay modes. To suppress the combinatorial background, we impose a selection on the scaled momentum $x_p = p^*/\sqrt{s/4 - m^2} > 0.5$, where p^* is the momentum of a Ξ_{cc} candidate in the center-of-mass frame (CM), s denotes the CM energy squared, and m is the mass of the Ξ_{cc} candidate.

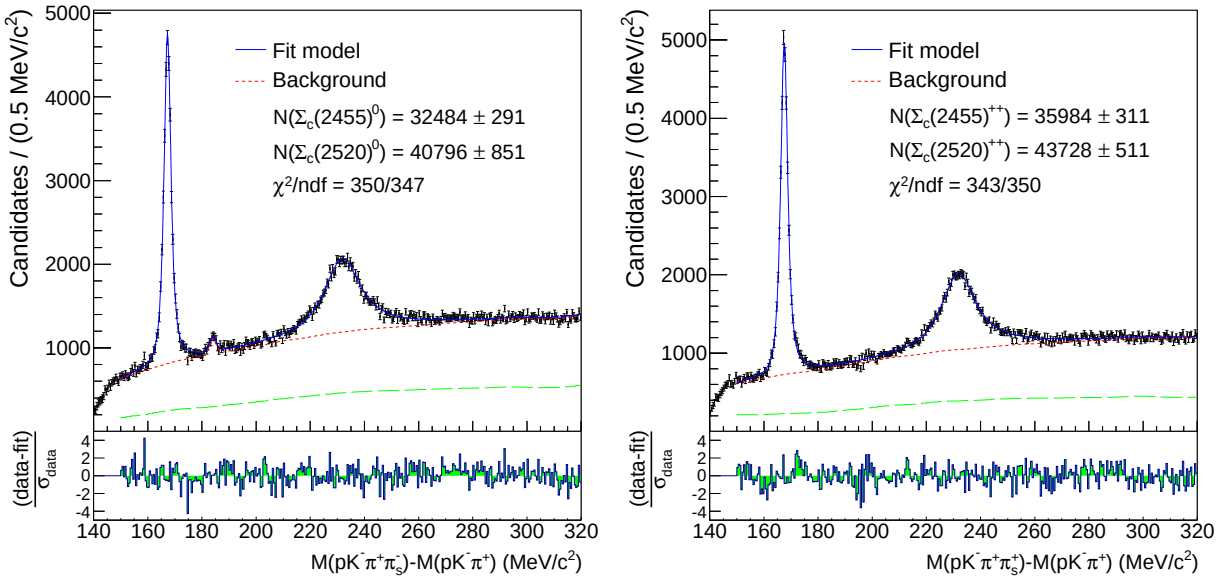

Figure 6: Fits to the mass differences $M(pK^-\pi^+\pi_s^-) - M(pK^-\pi^+)$ (left) and $M(pK^-\pi^+\pi_s^+) - M(pK^-\pi^+)$ (right) obtained from data (points with error bar) with the models (solid l ines) described in the text. The random backgrounds without true Λ_c^+ baryons (long-dashed line) and the total backgrounds (dashed lines) are shown as well. The peak near 185 MeV/c^2 in the left plot is due to the $\Xi_c^0 \to \Lambda_c^+\pi^-$ decay. The fit signal yields as well as th e fit χ^2 per degree of freedom are indicated on the plots. The bottom histograms are the differences between the values of data and fit divided by the statistical uncertainties of data to illustrate the fit quality.

Table 2: The measurements of the masses (M_0) and the widths (Γ) of the $\Sigma_c(2455)^{0/++}$ and $\Sigma_c(2520)^{0/++}$ baryons. The first error is statistical and the second is systematic. The masses are calculated by adding the world average of Λ_c^+ mass to the mass differences (ΔM_0) and the third error is the total uncertainty of the world average of Λ_c^+ mass [6].

	ΔM_0 (MeV/c^2)	Γ (MeV/c^2)	M_0 (MeV/c^2)
$\Sigma_c(2455)^0$	$167.29 \pm 0.01 \pm 0.02$	$1.76 \pm 0.04^{+0.09}_{-0.21}$	$2453.75 \pm 0.01 \pm 0.02 \pm 0.14$
$\Sigma_c(2455)^{++}$	$167.51 \pm 0.01 \pm 0.02$	$1.84 \pm 0.04^{+0.07}_{-0.20}$	$2453.97 \pm 0.01 \pm 0.02 \pm 0.14$
$\Sigma_c(2520)^0$	$231.98 \pm 0.11 \pm 0.04$	$15.41 \pm 0.41^{+0.20}_{-0.32}$	$2518.44 \pm 0.11 \pm 0.04 \pm 0.14$
$\Sigma_c(2520)^{++}$	$231.99 \pm 0.10 \pm 0.02$	$14.77 \pm 0.25^{+0.18}_{-0.30}$	$2518.45 \pm 0.10 \pm 0.02 \pm 0.14$

Figure 7 (a) and (b) show the $M(\Lambda_c^+K^-\pi^+)$ and $M(\Lambda_c^+K^-\pi^+\pi^+)$ distributions, respectively. No significant signal is found in the data for either Ξ_{cc}^+ or Ξ_{cc}^{++}. The statistical significance for a given mass is evaluated with an unbinned extended maximum likelihood fit. The probability density function for the signal is described with signal MC generated for each given Ξ_{cc} mass, whereas a third-order polynomial function is used for the background. The statistical significance is defined as $\sqrt{-2\ln(\mathcal{L}_0/\mathcal{L})}$, where $\mathcal{L}_0$ is the maximized likelihood value from the fit with the signal yield set at 0 and $\mathcal{L}$ is the best fit value with the signal yield floated. The significance is evaluated for the Ξ_{cc} mass scanned with a 1 MeV/c^2 step in the search region and the 95% C.L. upper limits for $\sigma_{\mathcal{B}}$ are shown in 7 (c) and (d) for Ξ_{cc}^+ and Ξ_{cc}^{++}, respectively.

We perform a search for the excited Ξ_c^+ (Ξ_c^{*+}). Here, we require x_p to be greater than 0.7 which can be compared with the reported BABAR selection $p^*(\Lambda_c^+K^-\pi^+)$ >2.9 GeV/c, shown in Fig. 8 (a). Figure 8 (b) shows the $M(\Lambda_c^+\pi^+)$ distribution, where contributions from the $\Sigma_c(2455)^{++}$ and the $\Sigma_c(2520)^{++}$ baryons are clearly visible. We select the $\Sigma_c(2455)^{++}$ ($\Sigma_c(2520)^{++}$) region by requiring $|M(\Lambda_c^+\pi^+) - m_{\Sigma_c^{++}}| <$ 5 (18) MeV/c^2, where $m_{\Sigma_c^{++}}$ is the nominal mass of the $\Sigma_c(2455)^{++}$ or $\Sigma_c(2520)^{++}$. Figure 8 (c) shows the $M(\Lambda_c^+K^-\pi^+)$ distribution for the $\Sigma_c(2455)^{++}$ signal region together with the same plot for the $\Sigma_c(2455)^{++}$ sideband region, defined as $|M(\Lambda_c^+\pi^+) - m_{\Sigma_c(2455)^{++}} \pm 15$ MeV/c^2 | < 5 MeV/c^2. Clear peaks corresponding to the $\Xi_c(2980)^+$, $\Xi_c(3055)^+$ and $\Xi_c(3080)^+$ are seen. The fit curve with Breit-Wigner functions convolved with detector response function for resonances and threshold function for background is also shown. The observation of $\Xi_c(3055)^+$ confirms the reported evidence [9] by the BABAR collaboration. Figure 8 (d) shows the $M(\Lambda_c^+K^-\pi^+)$ distribution for the $\Sigma_c(2520)^{++}$ selected region together with the same plot for the $\Sigma_c(2520)^{++}$ sideband region, defined as $|M(\Lambda_c^+\pi^+) - m_{\Sigma_c(2520)^{++}} \pm 27$ MeV/c^2 | < 12 MeV/c^2. A clear peak corresponding to the $\Xi_c(3080)^+$ is seen, while no peaking structure is found in the mass near 3.123 GeV/c^2 as reported by BABAR [9].

5. Exclusive $\Lambda\bar{\Lambda}$ production at $\Upsilon(1S, 2S)$

Significant enhancements in the inclusive production of hyperons from $\Upsilon(nS) \to ggg$ were found with respect to $e^+e^- \to q\bar{q}$. It is of theoretical interests to understand the production mechanism. However, studies of baryon-antibaryon pair production have never been explicitly pursued for bottomonium states although such incidence like antideuteron, a bound state of antiproton and antineutron, already exists.

The Belle collaboration used the collected $\Upsilon(1S)$ and $\Upsilon(2S)$ data samples for this study. The integrated luminosity is 5.8 fb^{-1} and 21.3 fb^{-1} for $\Upsilon(1S)$ and $\Upsilon(2S)$, respectively. We exclusively reconstruct $\Upsilon(1S, 2S) \to \Lambda\bar{\Lambda}X$, where X can be $\pi^+\pi^-$, K^+K^-, $\pi^+\pi^-\pi^0$, $K^+K^-\pi^0$, $\pi^+\pi^-\pi^+\pi^-$, $K^+K^-\pi^+\pi^-$, ... upto 7 final-state mesons with at most one π^0. The signal yield is determined by a fit to the spectrum of total reconstructed hadron energy. The continuum peaking contribution is properly subtracted by comparing the Onpeak and Offpeak data samples. The measured branching fractions are of the order of 10^{-6} - 10^{-5} with a trend that higher multiplicities in the final state have bigger branching fractions. There is an interesting feature of the observed $\Lambda\bar{\Lambda}$ mass spectra which all show significant enhancement near $\Lambda\bar{\Lambda}$ mass threshold. The same phenomenon has been observed before, for example, in $B^+ \to \Lambda\bar{\Lambda}K^+$ decays [10].

Acknowledgments

The author wish to thank the organizers for hosting such a wonderful conference. This work is supported by the National Science Council of the Republic of China under the grant NSC-102-2112-M-002-015.

References

[1] J.P. Lees *et al.*, Phys. Rev. D **89**, 111102 (2014).
[2] R. Giles *et al.*, Phys. Rev. D **29**, 1285 (1984).
[3] R. Hagedorn, Nucl. Phys. B **24**, 93 (1970).
[4] A. Zupanc *et al.*, Phys. Rev. Lett. **113**, 042002 (2014).
[5] Hereafter, the inclusion of the charge conjugate mode is implied.
[6] J. Beringer *et al.* (Particle Data Group), Phys. Rev. D **86**, 010001 (2012).
[7] S.-H. Lee *et al.*, Phys. Rev. D **89**, 091102 (2014).
[8] Y. Kato *et al.*, Phys. Rev. D **89**, 052003 (2014).
[9] B. Aubert *et al.* [BaBar Collaboration], Phys. Rev. D **77**, 012002 (2008)
[10] Y.J. Lee *et al.*, Phys. Rev. Lett. **93**, 211801 (2004).

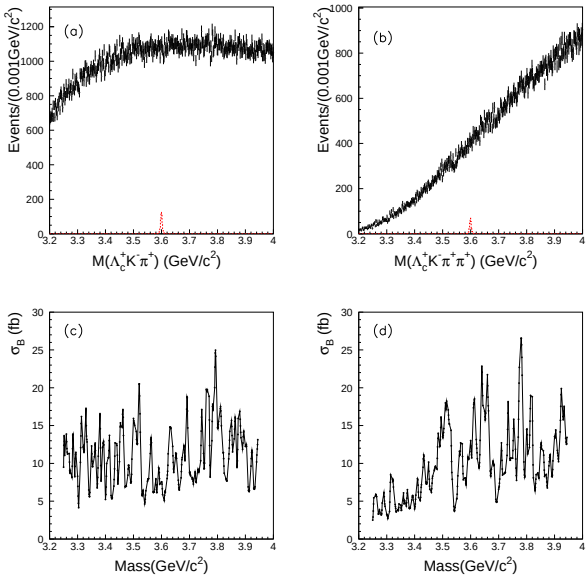

Figure 7: Invariant mass distribution of the Ξ_{cc} candidates for (a) $M(\Lambda_c^+K^-\pi^+)$, (b) $M(\Lambda_c^+K^-\pi^+\pi^+)$; the vertical error bars are from data and the dashed histogram are from signal MC for the Ξ_{cc} signal generated with a mass of 3.60 GeV/c^2 and a production cross section $\sigma(e^+e^- \to \Xi_{cc}^{+(+)}X)$ of 500 fb and $\mathcal{B}(\Xi_{cc}^{+(+)} \to \Lambda_c^+K^-\pi^+(\pi^+))$ of 5%. 95% C.L. upper limit of $\sigma_{\mathcal{B}}$ as a function of the mass with a 1 MeV/c^2 step for (c) Ξ_{cc}^+ and (d) Ξ_{cc}^{++}.

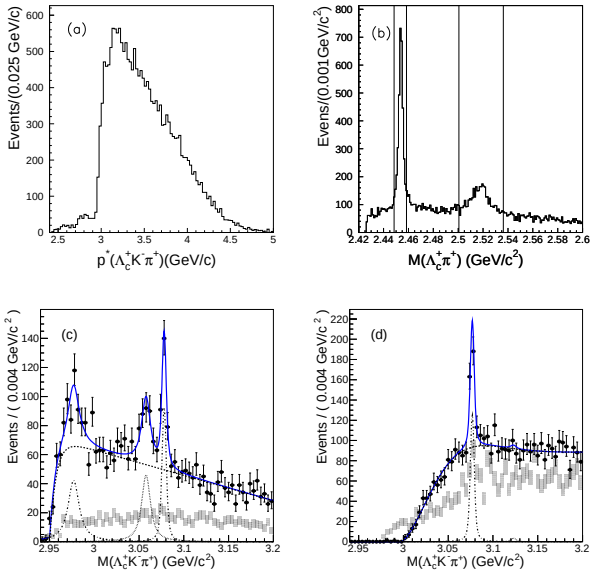

Figure 8: (a) The $p^*(\Lambda_c^+K^-\pi^+)$ distribution from data. (b) The $M(\Lambda_c^+\pi^+)$ distribution. The vertical lines show the selected regions of the $\Sigma_c(2455)^{++}$ and $\Sigma_c(2520)^{++}$. (c) The $M(\Lambda_c^+K^-\pi^+)$ distribution with $\Sigma_c(2455)^{++}$ selection. The dots with error bars show the distribution for the $\Sigma_c(2455)^{++}$ selected region whereas the rectangles show the distribution for the $\Sigma_c(2455)^{++}$ sideband region. The solid line shows the fit result. The dashed, dotted, and dash-dotted lines show the contributions from the background, $\Xi_c(3055)^+$, and $\Xi_c(2980)^+$ or $\Xi_c(3080)^+$, respectively. (d) The $M(\Lambda_c^+K^-\pi^+)$ distribution with $\Sigma_c(2520)^{++}$ selection. The dots with error bars show the distribution for $\Sigma_c(2520)^{++}$ selected region whereas the rectangles show the distribution for the $\Sigma_c(2520)^{++}$ sideband region. The solid line shows the fit result. The dashed, dotted, and dash-dotted lines show the contributions from the background, $\Xi_c(3123)^+$, and $\Xi_c(3080)^+$, respectively.